

# Feature-Align Network and Knowledge Distillation for Efficient Denoising

Lucas D. Young\*  
Jon Morton  
Xiaoyu Xiang

Fitsum A. Reda\*<sup>†</sup>  
Jun Hu  
David Liu  
Facebook Inc.

Rakesh Ranjan  
Yazhu Ling  
Vikas Chandra

## Abstract

Deep learning-based RAW image denoising is a quintessential problem in image restoration. Recent works have pushed the state-of-the-art in denoising image quality. However, many of these networks are computationally too expensive for efficient use in mobile devices. Here, we propose a novel network for efficient RAW denoising on mobile devices. Our contributions are: (1) An efficient encoder-decoder network augmented with a new Feature-Align layer to attend to spatially varying noise. (2) A new perceptual Feature Loss calculated in the RAW domain to preserve high frequency image content. (3) An analysis of the use of multiple models tuned to different subranges of noise levels. (4) An open-source RAW noisy-clean paired dataset with noise modeling, to facilitate research in RAW denoising. We evaluate the effectiveness of our proposed network and training techniques and show results that compete with the state-of-the-art network, while using significantly fewer parameters and MACs. On the Darmstadt Noise Dataset benchmark, we achieve a PSNR of 48.28dB, with  $263\times$  fewer MACs, and  $17.6\times$  fewer parameters than the state-of-the-art network, which achieves 49.12 dB.

## 1. Introduction

Image acquisition is inevitably contaminated by noise due to various environmental effects. For instance, low-light imaging under a high ISO setting may yield noisy images. Noise in images not only degrades perceptual quality, but may also compromise the effectiveness of subsequent computer vision tasks. Noisy images are especially prevalent in everyday devices, such as smartphones and wearables, which often have small sensors and limited light intake ability.

Image denoising is a classical yet actively studied topic in image restoration [9, 6, 10, 12, 35, 36]. Recent at-

\*Equal contribution.

<sup>†</sup>Currently affiliated with Google.

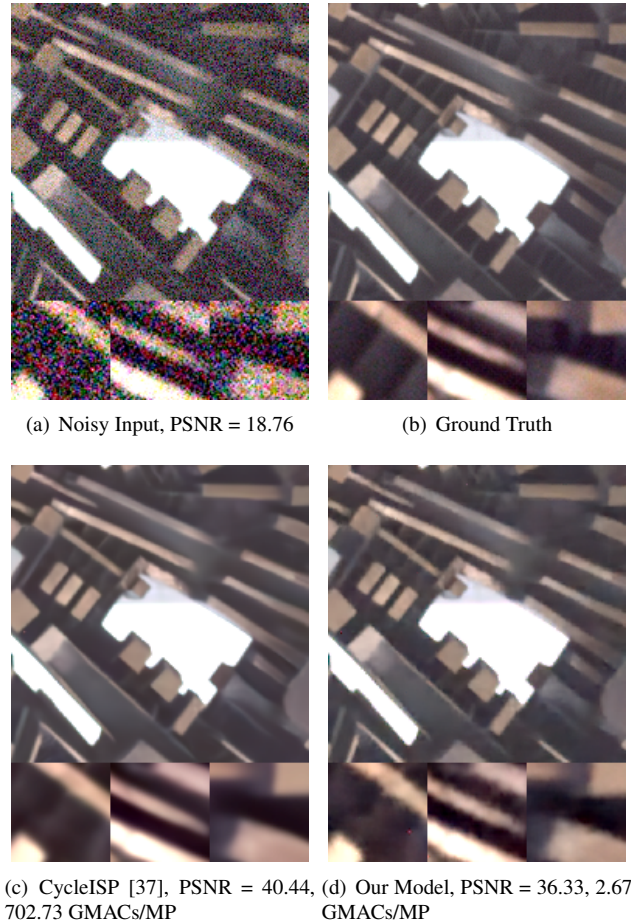


Figure 1. Our efficient denoising method compared to the existing state-of-the-art denoising method, CycleISP when applied to an image in the Darmstadt Noise Dataset [28]. Our method produces similar results with  $263\times$  fewer MACs.

tention for the problem focuses on applying deep neural networks to RAW sensor data or to images obtained after post-processing with the device’s image signal processor (ISP) [33, 26, 38, 17, 40, 27]. For instance, [33] proposes

a generalized residual dense network with 22M parameters. [26] combines a multi-level wavelet residual network with a progressive training scheme and achieves a run time of 364 milliseconds per mega-pixel (MP). These networks are often computationally too expensive to run at real-time on edge devices.

In this work, we introduce an efficient neural network for high quality RAW denoising. We build upon the U-Net architecture [29] to realize our model. While the success of the U-Net architecture has been celebrated in learning complex mappings for several dense prediction tasks, such as semantic segmentation, depth estimation or image synthesis, its direct deployment on mobile devices with limited compute-budget is not optimal. Trivial reduction of U-Net parameters is not sufficient to learn robust models. As such, recent works have focused on efficient blocks to replace key building blocks of the U-Net architecture, such as MobileNet and its variants, Shuffle Nets, and Squeeze Nets. In this work, we adapt these key building blocks and present new architectural changes to boost the learning ability of light-weight U-Net architectures for RAW denoising tasks. We examine the use of multiple efficient models to tackle a wide problem space despite the limited number of learned parameters in the efficient model. We also introduce a novel perceptual loss function aimed at restoring fine image details obscured by high noise. In summary, the primary contributions of this paper are:

- A novel model architecture with the Feature Align layer for efficient image denoising.
- A novel perceptual loss function and method for knowledge distillation, the Feature Loss, aimed at maximizing texture recovery in image denoising.
- An analysis of the use of multiple networks trained for different noise levels.
- An open-source dataset of RAW Sony IMX258 images with accompanying ground truths and noise-level annotations.

## 2. Related Work

Single-frame image denoising is a fundamental problem in image processing and computer vision. Prior methods such as BM3D [9] and non-local means [6] rely on hand-engineered algorithms [10, 12, 35, 36]. With the introduction of data-driven neural network-based methods [33, 26, 38, 17, 40, 27], datasets pairing noisy images to noise-free images became sought after [1, 8, 2]. However, it is well known and demonstrated in public benchmarks that denoising RAW image data yields superior results when compared to denoising images after being processed by the ISP [28]. Because of the construction difficulty and limited availability of paired noisy and clean RAW images,

other works have reduced data collection needs by simulating noisy images by adding white gaussian noise (AWGN) to noise-free images. Recent works observe that true sensor noise exhibits characteristics unlike AWGN, and thus they propose robust noise modeling mathematics by considering the physical properties of sensors [5, 28, 34, 4, 14, 13, 11]. UPI [5] and CycleISP [37] further synthesize RAW images from real-life RGB images by inverting the ISP pipeline. By exploiting several public RGB image datasets, such as MIR-FLICKR [16], and modeling artificial noise, CycleISP and UPI increase the size of paired RAW datasets, demonstrating state-of-the-art performance on a public benchmark, suggesting the generalizability of this approach.

[21] observes that denoising model performance can be improved by horizontal and vertical flipping augmentations of training data. However, naive implementations of the flipping operations on RAW data can yield artifacts after postprocessing. [21] proposes altered flipping operations for RAW data that do not yield artifacts after postprocessing. Additionally, it observes that switching channels of RAW data to emulate a different Bayer pattern also yields artifacts after postprocessing. It proposes an alternative to this operation that enables sourcing training data from sensors with different Bayer patterns without introducing artifacts.

While these works introduce valuable techniques for denoising, they do not study less computationally expensive variants of their methods. PMRID [34], the most similar work to ours, is the first to address this disparity in neural denoising. Specifically, it introduces an efficient model architecture using separable convolutions. It also builds upon the variance stabilizing transform [3, 24] by introducing the k-sigma transform, which normalizes data such that per-pixel variance is not dependent on the ISO of the exposure. PMRID also describes a noise modeling method similar to UPI. While the work we propose here shares similar goals to PMRID, a one-to-one comparison can not be performed as PMRID’s networks weights or test datasets are not publicly available at the time of this paper’s writing.

Our proposed technique builds upon previous works, and particularly incorporates the following prior techniques:

- Noise modeling of our target camera’s sensor, Sony IMX258, with a method similar to PMRID and UPI, to add realistic artificial noise to ground truths.
- Unprocessing [5] the MIRFLICKR-1m [16] dataset to create a large RAW training dataset.
- Incorporation of Bayer Augmentation [21] in our training pipeline.
- Use of Bayer Unification [21] to use ground truths from the sensors in the SIDD [1] and SID [8] dataset.

- Incorporation of the k-sigma transform [34]

Lastly, we take inspiration from a method traditionally applied to superresolution, perceptual loss [19], in the creation of our novel Feature Loss function.

### 3. Method

Given a noisy RAW image  $\mathbf{I}_n$ , we aim to learn efficient neural networks to denoise and produce clean RAW image  $\tilde{\mathbf{I}}$ , in a data-driven way. Mathematically, the denoising problem is formulated as,

$$\tilde{\mathbf{I}} = \mathcal{F}(\mathbf{I}_n), \quad (1)$$

where  $\mathcal{F}$  is an efficient neural network we aim to learn. Due to the scarcity of large scale paired RAW training images, we conduct our training by constructing a large scale of synthetic pairs of clean and noisy RAW images. In a similar setup to [5, 34], a noisy image is synthesized by a simple addition of noise  $\mathbf{n}$  sampled from a noise model to a clean RAW image  $\mathbf{I}$ . We rely on clean RAW images obtained by either unprocessing real-life RGB images, or from publicly available clean RAW sensor datasets. Note that the RGB images we present here to visually motivate or validate our methods are obtained after processing the denoised RAW image  $\tilde{\mathbf{I}}$  with the camera ISP. We use  $\mathbf{I}^f$  and  $\tilde{\mathbf{I}}^f$  to denote the final noisy RGB image and final denoised RGB image respectively.

#### 3.1. Model Architecture

We realize our neural network  $\mathcal{F}$  with a U-Net-like architecture. U-Net-like models have been extensively studied for various computer vision tasks. Most of these works employ large and computationally expensive models. Our work proposes a light-weight and efficient U-Net-like model for RAW denoising. We also propose techniques to boost the learning ability of such light-weight models. In particular, we make the following architectural changes to the U-Net model: 1) To achieve efficient learning, we replace the convolutional layers with a variant of the MobileNet-V2 block [30]. 2) To reduce the memory footprint of skip layers, we introduce shrunk skip-connection, implemented with a point-wise convolution. 3) To reduce the "washing away" phenomenon of important image features in model learning, as pointed out in the SPADE architecture, we introduce a new Feature-Align layer. The following subsections describe each design choice. Figure 4 illustrates our proposed efficient architecture.

**A variant of MobileNet-V2 block:** A typical U-Net architecture consists of a contracting and an expanding set of layers. In efficient learning, these layers are often realized with well studied efficient blocks such as MobileNet-V1, MobileNet-V2 etc. In this work, we use a variant of the MobileNet-V2 efficient block to realize each layer in our

U-Net. Specifically, as illustrated in Figure 2, we replace MobileNet-V2's depth-wise convolution with a group convolution for improved compute vs accuracy trade-off.

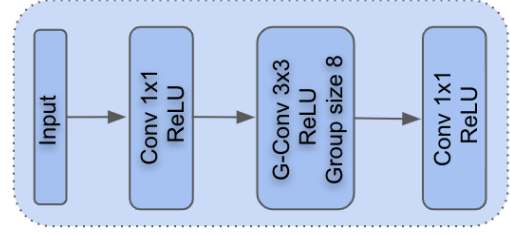


Figure 2. ARNet-block, a variant of MobileNet-V2 [30]

**Shrunk Skip Connections:** Skip-connections in a U-Net architecture allow processing of multi-scale features. High-resolution features from the contracting layers are combined with low-resolution features from the expanding layers in the decoder layer, with addition, concatenation or other forms of feature fusion. In memory constrained devices, storing encoder activations until their processing by decoder layers is not desirable. To alleviate this limitation, as illustrated in Figure 4, we apply a point-wise convolution to shrink the encoder features. At the decoder layer, we replicate the contracted features to match the size of the expanding features to perform fusion operations.

**Input Feature-Align Layer:** Prior neural network-based denoising techniques take in noisy inputs and directly process them through a sequence of convolution and non-linearity layers. While this is also a common technique for various dense prediction tasks, in our experiments, we observed such direct processing to bias our light-weight models to exhibit global over- or under-denoising. As shown in our experiments, we attribute this to the recently studied phenomenon of "washing away" of input details during processing with a stack of multi-scale layers. In our case, we tightly integrate the input noisy information at each layer of our network with a Feature-Align layer, to enable our models to learn to denoise images in a spatially adaptive manner.

Let  $\mathbf{F}^i \in \mathbb{R}^{N \times C^i \times H^i \times W^i}$  denote the feature map of layer  $i$ , with  $N, C^i, H^i, W^i$  being the batch size, channel count, height and width, respectively, of the feature map. Our Feature-Align layer, in a similar way as a Batch Norm layer, or the Spatially-Adaptive De-normalization (SPADE) layer, applies a scale and a bias to affinely transform the inputs, guided by the noisy input image. Specifically, we compute the pixel-wise scale and bias parameters based on the noisy input image, as illustrated in Figure 3. Mathematically, the affine transformation of a feature map is given by

$$\mathbf{G}^i = \gamma^i \cdot \mathbf{F}^i + \beta^i, \quad (2)$$

with  $\gamma^i \in \mathbb{R}^{N \times C^i \times H^i \times W^i}$  and  $\beta^i \in \mathbb{R}^{N \times C^i \times H^i \times W^i}$  being

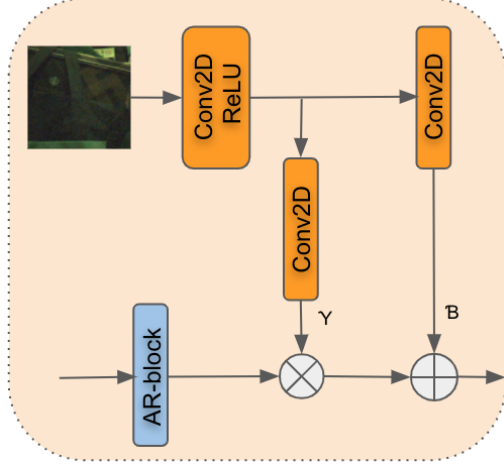


Figure 3. Input Feature-Align Layer, inspired by the SPADE architecture [25]

the scale and bias parameters that are a function of the input noisy image.

### 3.2. Loss functions

**Charbonnier Loss:** Our primary loss function is the Charbonnier Loss [7] over the denoised image, given by

$$\mathcal{L}_{charb} = \sqrt{(\tilde{\mathbf{I}} - \mathbf{I})^2 + c^2} \quad (3)$$

where  $c$  is a constant parameter ( $1e - 6$  in our implementation).

**RGB Perceptual Loss:** UPI [5] describes a variant of their network in which training loss is computed after postprocessing the predicted image and ground truth with a minimalist ISP implementation. This incentivizes the network to predict RAW images that closely match the ground truth after postprocessing, rather than optimize for RAW signal fidelity. We expand upon this idea with the RGB Perceptual Loss, in which a perceptual loss such as that described in [19] is computed upon the predicted image and ground truth after postprocessing. After the postprocessing step, the implementation is identical to that of [19]; the loss is defined as the difference between  $\tilde{\mathbf{I}}^f$  and  $\mathbf{I}^f$  in content and style in activations of a pretrained VGG16 classification network [32] trained on ImageNet.

**Simple Knowledge Distillation:** The additional layers of conventional larger networks can enable the model to encode image features at a higher, more perceptual level and make imaginative judgments to “fill in the blank” of a missing texture obscured by noise. Since this capability is diminished with smaller networks, image outputs from efficient networks are prone to appear oversmoothed. As a result, knowledge distillation [15] is applicable to the challenge of creating an efficient model with perceptually pleasing image outputs.

Another observation from experimenting with a large denoising model (the same U-Net architecture used in [5]) is that if a noise-free image is fed to the network as an input, the output is virtually unaltered. This observation enables a simple implementation of knowledge distillation in the form of a loss function defined as the difference between the student network’s predicted image,  $\tilde{\mathbf{I}}_{student}$  and the large teacher network’s predicted image,  $\tilde{\mathbf{I}}_{teacher}$ :

$$\mathcal{L}_{k.d.} = |\tilde{\mathbf{I}}_{student} - \tilde{\mathbf{I}}_{teacher}| \quad (4)$$

**Feature Loss for Knowledge Distillation:** Expanding on Simple Knowledge Distillation and perceptual loss, our novel Feature Loss implements knowledge distillation in the form of a perceptual loss function. The Feature Loss is defined as the difference in content and style between the activations of the teacher network on the predicted image and the ground truth image. The implementation is identical to [19], except the classifier model is substituted for the teacher network. By combining knowledge distillation with perceptual loss, the capability of large networks to recover fine details obscured by noise is specifically targeted for distillation.

### 3.3. Noise Subrange Model Array

The number of parameters in our efficient model architecture is limited in comparison to large model architectures traditionally used for neural denoising. In contrast, the problem space widely ranges from minimal noise to extreme noise, requiring vastly different denoising strategies depending on the noise level. With a limited number of parameters, it is challenging to create a model that optimally responds to every possible noise level. Thus, we offer the strategy of a Noise Subrange Model Array (NSMA), in which the range of noise levels is partitioned into  $n$  subranges where an individual model is trained for each noise subrange. To partition the noise levels, we refer to the regression between  $\log a$  and  $\log b$  in Figure 2 of the supplemental material and partition the x-axis into  $n$  parts. Given the global minimum signal dependent noise parameter,  $a_{min}$ , and global maximum signal dependent noise parameter  $a_{max}$ , Equation 5 and 6 describe the minimum and maximum  $a$  parameters for artificial noise in training for the zero-indexed  $i$ th model in the array of  $n$  models.

$$\log a_{min_i} = \log a_{min} + i/n \cdot (\log a_{max} - \log a_{min}) \quad (5)$$

$$\log a_{max_i} = \log a_{min} + (i + 1)/n \cdot (\log a_{max} - \log a_{min}) \quad (6)$$

In testing, we observe the annotated  $a$  parameter of the image and select the corresponding model from the model array.



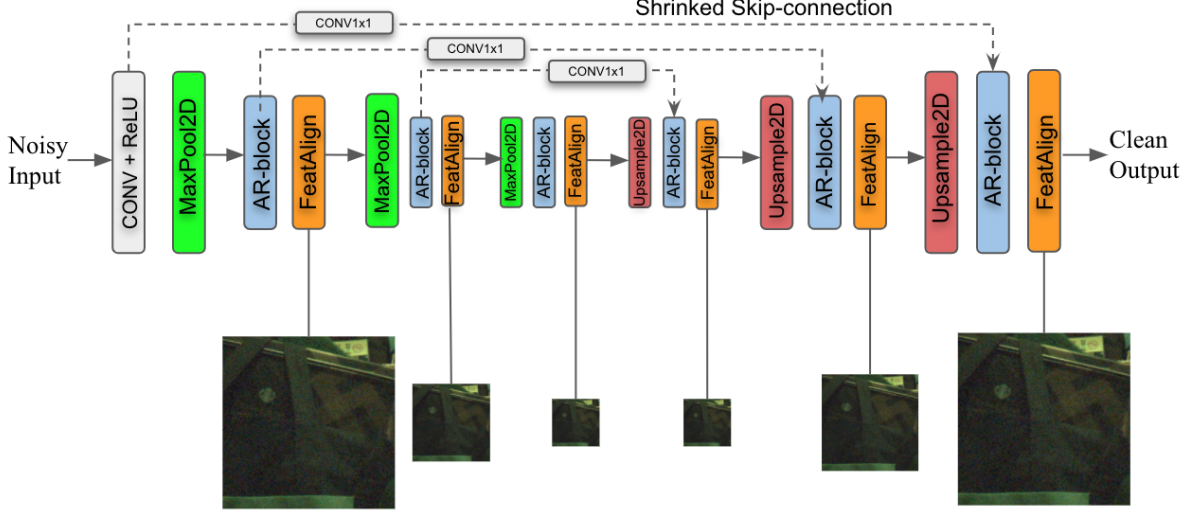


Figure 4. Our U-Net-based model architecture. Shrunked skip-connections combine high-resolution features in encoding layers with low-resolution features in decoder layers. A Feature-Align layer combines the original input features at different resolutions with the output for each efficient ARNet block.

### 3.4. Training and Implementation Details

To train our array of models we use the following configuration:

- The training ground truth images consist of unprocessed MIRFLICKR [16] with modified white balance gains, SIDD [1], and the Learning to See in the Dark training dataset [8]. The latter two datasets are unified into an RGGB pattern with Bayer Unification [21]. These images are randomly cropped into 128 x 128 patches.
- Bayer Augmentation [21] is applied to the training data.
- The input to the model is generated by adding artificial noise to the ground truth image. A description of our experiments to realistically model artificial noise is included in supplemental Section 6.
- The k-sigma transform of [34] is implemented in training and testing. Note that  $k$  and  $\sigma^2$  refer to our  $a$  and  $b$  noise parameters respectively.
- Training examples are collated into batches of size 16.
- The Charbonnier Loss variant of our models uses a loss weight of 393.5. The Feature Loss variant of our models uses a loss weight of 78.7. These weights were derived from a hyperparameter sweep on RAW PSNR.
- Models are trained using the Adam [20] optimizer with the maximum learning rate of  $1e-4$ .
- Training occurs in 2,500,000 iterations scheduled with cosine learning rate decay.

### 3.5. Datasets and Metrics

We train our method by adding artificial noise to RAW ground truth images as detailed in Section 3.4. While our denoising network is trained with artificial noise, we test our network with real noise. We contribute the publicly available Feature Align Paired Test Dataset of noisy RAW images paired with corresponding noise-free ground truths. We collect these image pairs on the targeted camera of our method which uses a Sony IMX258 sensor. Pairs are collected by taking a short exposure with a random gain between 1.0 and 64.0 accompanied by a long exposure of the same scene with a gain of 1.0. The long exposure’s exposure time is adjusted such that the brightness of both images are equivalent. The gain and exposure time is selected programatically so that the camera is not moved slightly between image captures. Similar to the Darmstadt Noise Dataset [28], to account for small environmental vibrations occurring between the short and long exposure that misalign the pair, we predict and correct for a global 2D translation estimated by averaging the Lucas-Kanade [23] optical flow of features detected by the Shi-Tomasi [18] algorithm. Finally, noise level annotations  $a$  and  $b$  for the short exposure are estimated from the regression described in supplemental Section 6.

## 4. Results

### 4.1. Experiments

In this section we evaluate denoising results of various experiments using the paired noisy and ground truth test set described in Section 3.5. We evaluate our results using tra-

ditional metrics for image quality, PSNR and SSIM, both before and after processing the images using the minimalist ISP pipeline from [5] with modified white balance gains for our sensor. We also evaluate our results qualitatively against the ground truth image. To display texture preservation, all images are zoomed in to the same highly textured region of an image in the test set. To examine the computational efficiency of networks we quantify the number of multiply-accumulate operations (MACs) required by the network.

Table 1 compares our Feature-Align method against a similarly sized model that uses the wavelet transform in up-sampling and downsampling as a baseline to approximate the prior state-of-the-art [22, 31]. To simplify the comparison, the Noise Subrange Model Array is not used in this experiment. A plain U-Net that does not include the wavelet transform or the Feature-Align layer, along with the Feature-Align model with shrunk skip connections removed are also included in the comparison. With traditional metrics, the Feature-Align model performs virtually equivalent to the wavelets model. Qualitatively, the Feature-Align model shows sharper edges and less blurring of fine details. To show additional generalization of the Feature-Align layer, we compare the wavelet transform model to the Feature-Align model on collected noisy RAW Google Pixel-4 inputs in Figure 5. We note that the qualitative benefits of the Feature-Align layer are more easily observed on our Pixel-4 inputs than our paired test dataset. Furthermore, the Feature-Align model without shrunk skip connections performs the worst among the 4 networks. This indicates that the Feature-Align layer is not redundant to the shrunk skip connections despite the similarity of these techniques.

In Table 2 we examine the effect that the NSMA has on the Feature-Align model. The NSMA, which is comprised of 4 models, improves the model’s performance in every metric, while demonstrating greater recovery of texture qualitatively.

Using the Feature-Align model and NSMA, in Table 3 we compare the effect of altering the loss function. Since RGB Perceptual Loss, Simple Knowledge Distillation, and Feature Loss are targeted at perceptual image quality rather than pure signal fidelity, for a fair comparison we include the perceptual metric, LPIPS [39]. A lower LPIPS score indicates greater perceptual similarity. Simple Knowledge Distillation performs the best in the traditional PSNR and SSIM metrics, while Feature Loss performs the best in the LPIPS metric. Qualitatively, the outputs from the Feature Loss models are sharper and have the most texture present. Charbonnier Loss outperforms Feature Loss in the traditional metrics, demonstrating that the traditional metrics favor oversmoothing denoising strategies rather than texture recovering denoising strategies.

Figures 6 and 7 display a summary of our denoising improvements.

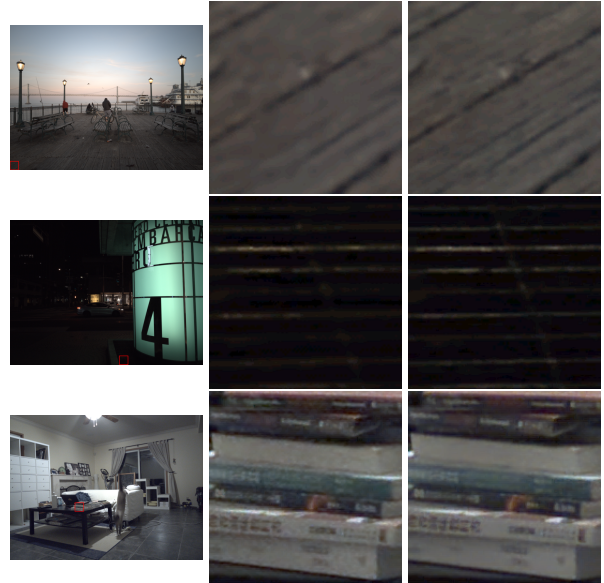


Figure 5. Left: Source image from Google Pixel-4. Red box highlights selected crop for comparison. Middle: Model output with wavelet transform. Right: Model output with our Feature-Align layer.

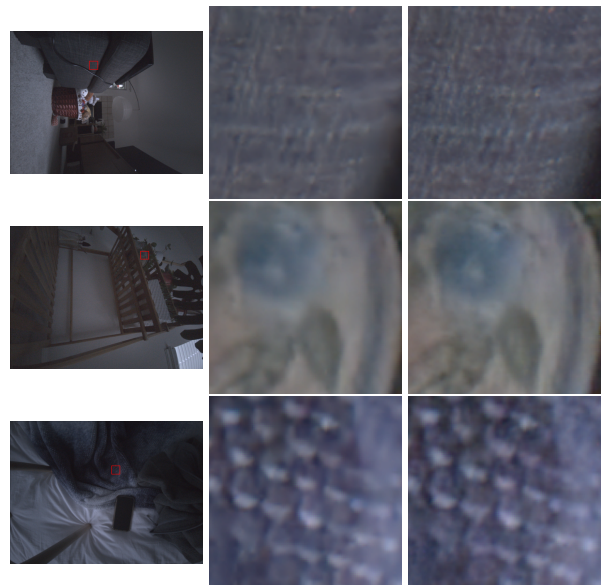


Figure 6. Summary of our improvements. Left: Source image. Red box highlights selected crop for comparison. Middle: Model output with wavelet transform, no NSMA, and Charbonnier Loss. Right: Model output with our Feature-Align layer, NSMA (n=4), and Feature Loss. Our method shows improved texture restoration.

Model Architecture Comparison					
Method	RAW PSNR	RAW SSIM	RGB PSNR	RGB SSIM	GMACs/MP
Input	36.616	0.80509	27.581	0.51557	-
Plain U-Net	45.485	0.97711	34.519	0.93481	2.2840
Wavelet	<b>45.576</b>	<b>0.97892</b>	<b>34.591</b>	0.93157	<b>1.9800</b>
Feature-Align	45.520	0.97780	34.565	<b>0.93491</b>	2.6688
FA w/o connections	45.395	0.97769	34.487	0.92534	2.5688

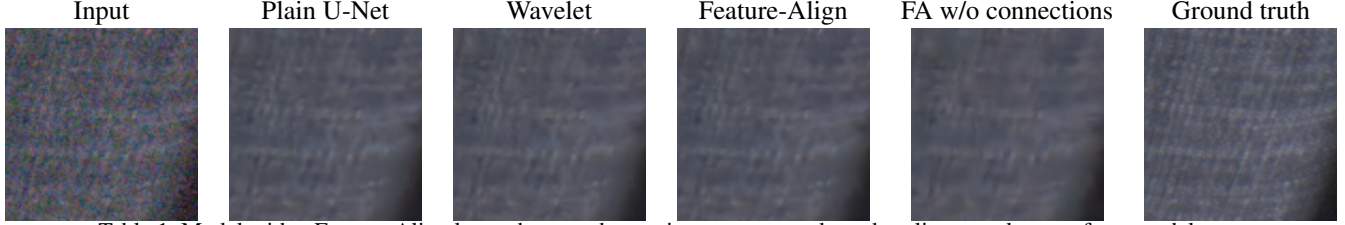


Table 1. Model with a Feature-Align layer shows a sharper image compared to a baseline wavelet transform model.

Effect of Noise Subrange Model Array				
Method	RAW PSNR	RAW SSIM	RGB PSNR	RGB SSIM
Input	36.616	0.80509	27.581	0.51557
No NSMA	45.520	0.97780	34.565	0.93491
NSMA (n=4)	<b>45.668</b>	<b>0.97936</b>	<b>34.869</b>	<b>0.94014</b>

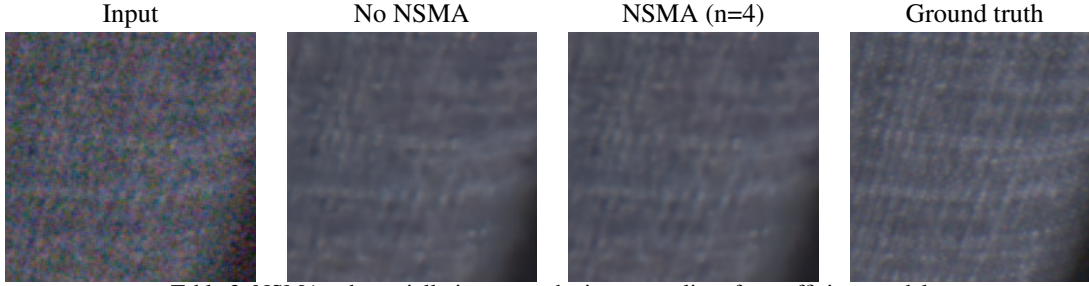


Table 2. NSMA substantially improves the image quality of our efficient model.

Effect of Loss Function					
Method	RAW PSNR	RAW SSIM	RGB PSNR	RGB SSIM	RGB LPIPS
Input	36.616	0.80509	27.581	0.51557	0.53680
Charbonnier	45.668	0.97936	34.869	0.94014	0.28882
RGB Perceptual	45.519	0.97685	34.665	0.92168	0.32448
Knowledge Dist.	<b>45.813</b>	<b>0.98217</b>	<b>35.499</b>	<b>0.94079</b>	0.27009
Feature	45.483	0.97828	34.607	0.93685	<b>0.24603</b>

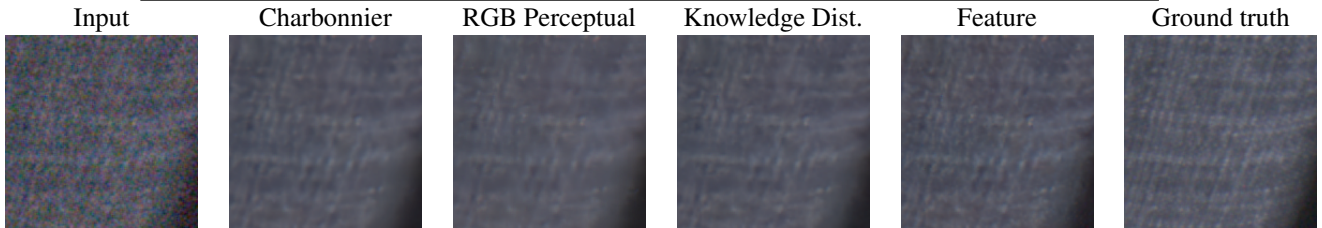


Table 3. Charbonnier Loss is outperformed by both Simple Knowledge Distillation and Feature Loss. Simple Knowledge Distillation has the best performance in traditional metrics, while Feature Loss has the best performance in the perceptual LPIPS metric. The model output with Feature Loss appears to have the most detail.



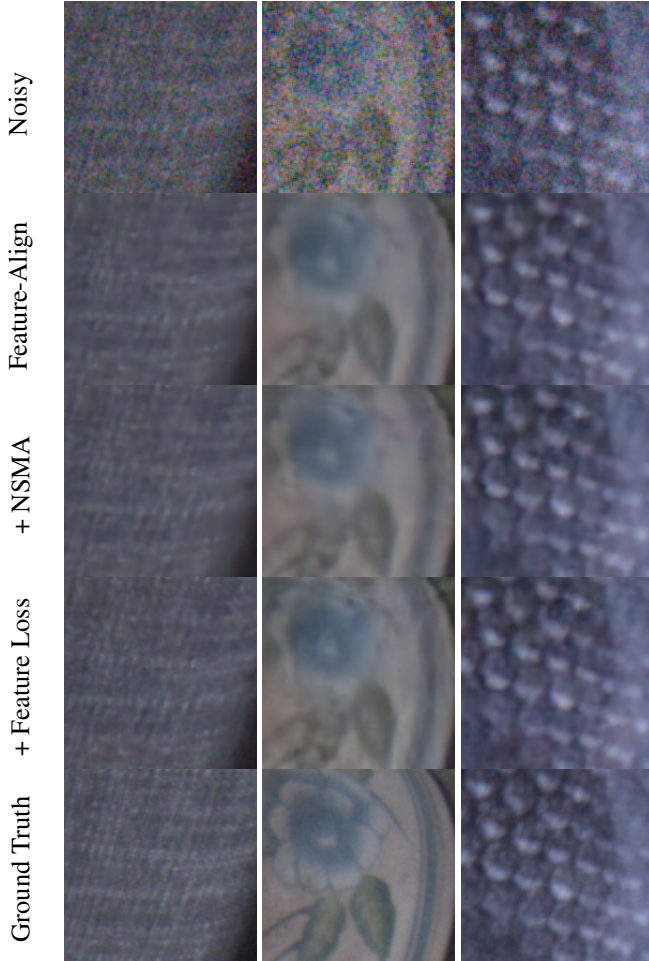


Figure 7. Our improvements in order: the effect of using the NSMA ( $n=4$ ) on our Feature-Align method, followed by the effect of replacing Charbonnier Loss with Feature Loss in the NSMA of Feature-Align models.

## 4.2. Generalization

For a standardized comparison of our method against existing state-of-the-art methods, we apply our method to the Darmstadt Noise Dataset public benchmark [28]. In training the noise parameters are tweaked to fit the DND test dataset and the white balance gains used to create the unprocessed MIRFLICKR dataset are tweaked to match [5] to be representative of DND. Table 4 shows our method compared to the top 3 submissions on the benchmark. Our method achieves a RAW PSNR of 48.2756, a comparable metric to the CycleISP’s [37] 49.1251 RAW PSNR, while using 263.32 times fewer MACs per megapixel. Our network uses 89,696 bytes of learned parameters, and the NSMA of 4 of our networks takes 4 times 89,696 bytes, which is 358,784 bytes. This is 22.7% the size of learned parameters used by CycleISP, 1,578,624 bytes.

Darmstadt Noise Evaluation					
Method	RAW PSNR	RAW SSIM	RGB PSNR	RGB SSIM	GMACs/MP
Noisy	-	-	29.836	0.7018	-
CycleISP	49.1251	0.983	40.4987	0.9655	702.73
UPI Raw	48.8905	0.9824	40.1728	0.9623	74.305
UPI RGB	48.8824	0.9821	40.3545	0.9641	74.233
Ours	48.2756	0.9808	39.5061	0.9572	2.6688

Table 4. Our method achieves comparable results to the computationally expensive state-of-the-art methods.

## 5. Conclusion

In this work we propose three innovations that enable high quality image denoising in an efficient model architecture: a Feature-Align layer, the use of an array of models tuned to different regions of the problem space, and a loss function for knowledge distillation that maximizes texture recovery. We combine these innovations along with existing state-of-the-art techniques and prove their efficacy by evaluating the method on a public benchmark. In addition, we propose a new public dataset of carefully constructed pairs of noisy and ground truth images with noise level annotations. The low computational cost of our method in comparison to existing state-of-the-art methods enables a variety of new applications for learning-based denoising in edge devices.



## References

- [1] Abdelrahman Abdelhamed, Stephen Lin, and Michael S. Brown. A high-quality denoising dataset for smartphone cameras. In *CVPR*, June 2018.
- [2] Josue Anaya and Adrian Barbu. Renoir – a dataset for real low-light image noise reduction. *Journal of Visual Communication and Image Representation*, 51:144–154, Feb 2018.
- [3] F. J. Anscombe. The transformation of poisson, binomial and negative-binomial data. *Biometrika*, 35(3/4):246–254, 1948.
- [4] L. Azzari and A. Foi. Gaussian-cauchy mixture modeling for robust signal-dependent noise estimation. In *2014 IEEE International Conference on Acoustics, Speech and Signal Processing (ICASSP)*, pages 5357–5361, 2014.
- [5] Tim Brooks, Ben Mildenhall, Tianfan Xue, Jiawen Chen, Dillon Sharlet, and Jonathan T. Barron. Unprocessing images for learned raw denoising. In *CVPR*, 2019.
- [6] H. C. Burger, C. J. Schuler, and S. Harmeling. Image denoising: Can plain neural networks compete with bm3d? In *CVPR*, pages 2392–2399, 2012.
- [7] P. Charbonnier, L. Blanc-Feraud, G. Aubert, and M. Barlaud. Two deterministic half-quadratic regularization algorithms for computed imaging. In *Proceedings of 1st International Conference on Image Processing*, volume 2, pages 168–172 vol.2, 1994.
- [8] Chen Chen, Qifeng Chen, Jia Xu, and Vladlen Koltun. Learning to see in the dark. In *CVPR*, 2018.
- [9] K. Dabov, A. Foi, V. Katkovnik, and K. Egiazarian. Image denoising by sparse 3-d transform-domain collaborative filtering. *IEEE Transactions on Image Processing*, 16(8):2080–2095, 2007.
- [10] Kostadin Dabov, Alessandro Foi, Vladimir Katkovnik, and Karen Egiazarian. Image restoration by sparse 3D transform-domain collaborative filtering. In Jaakko T. Astola, Karen O. Egiazarian, and Edward R. Dougherty, editors, *Image Processing: Algorithms and Systems VI*, volume 6812, pages 62 – 73. International Society for Optics and Photonics, SPIE, 2008.
- [11] Alessandro Foi. Clipped noisy images: Heteroskedastic modeling and practical denoising. *Signal Processing*, 89:2609–2629, 12 2009.
- [12] S. Gu, L. Zhang, W. Zuo, and X. Feng. Weighted nuclear norm minimization with application to image denoising. In *CVPR*, pages 2862–2869, 2014.
- [13] Samuel W. Hasinoff. *Photon, Poisson Noise*, pages 608–610. Springer US, Boston, MA, 2014.
- [14] S. W. Hasinoff, F. Durand, and W. Freeman. Noise-optimal capture for high dynamic range photography. *CVPR*, pages 553–560, 2010.
- [15] Geoffrey Hinton, Oriol Vinyals, and Jeff Dean. Distilling the knowledge in a neural network, 2015.
- [16] Mark J. Huiskes and Michael S. Lew. The mir flickr retrieval evaluation. In *MIR '08: Proceedings of the 2008 ACM International Conference on Multimedia Information Retrieval*, New York, NY, USA, 2008. ACM.
- [17] Y. I. Jang, Y. Kim, and N. I. Cho. Dual path denoising network for real photographic noise. *IEEE Signal Processing Letters*, 27:860–864, 2020.
- [18] Jianbo Shi and Tomasi. Good features to track. In *CVPR*, pages 593–600, 1994.
- [19] Justin Johnson, Alexandre Alahi, and Li Fei-Fei. Perceptual losses for real-time style transfer and super-resolution, 2016.
- [20] Diederik P. Kingma and Jimmy Ba. Adam: A method for stochastic optimization, 2017.
- [21] Jiaming Liu, Chi-Hao Wu, Yuzhi Wang, Qin Xu, Yuqian Zhou, Haibin Huang, Chuan Wang, Shaofan Cai, Yifan Ding, Haoqiang Fan, and Jue Wang. Learning raw image denoising with bayer pattern unification and bayer preserving augmentation, 2019.
- [22] Wei Liu, Qiong Yan, and Yuzhi Zhao. Densely self-guided wavelet network for image denoising. In *CVPRW*, June 2020.
- [23] Bruce D. Lucas and Takeo Kanade. An iterative image registration technique with an application to stereo vision. In *Proceedings of the 7th International Joint Conference on Artificial Intelligence - Volume 2, IJCAI'81*, page 674–679, San Francisco, CA, USA, 1981. Morgan Kaufmann Publishers Inc.
- [24] M. Makitalo and A. Foi. Optimal inversion of the anscombe transformation in low-count poisson image denoising. *IEEE Transactions on Image Processing*, 20(1):99–109, 2011.
- [25] Taesung Park, Ming-Yu Liu, Ting-Chun Wang, and Jun-Yan Zhu. Semantic image synthesis with spatially-adaptive normalization. In *CVPR*, pages 2337–2346, 2019.
- [26] Yali Peng, Yue Cao, Shigang Liu, Jian Yang, and Wangmeng Zuo. Progressive training of multi-level wavelet residual networks for image denoising. *arXiv preprint*, 2020.
- [27] Tobias Plötz and Stefan Roth. Neural nearest neighbors networks. In *Advances in Neural Information Processing Systems (NeurIPS)*, 2018.
- [28] Tobias Plötz and Stefan Roth. Benchmarking denoising algorithms with real photographs, 2017.
- [29] Olaf Ronneberger, Philipp Fischer, and Thomas Brox. U-net: Convolutional networks for biomedical image segmentation. In *CVPR*, 2015.
- [30] Mark Sandler, Andrew Howard, Menglong Zhu, Andrey Zhmoginov, and Liang-Chieh Chen. Mobilenetv2: Inverted residuals and linear bottlenecks. In *CVPR*, pages 4510–4520, 2018.
- [31] S. Sardy, P. Tseng, and A. Bruce. Robust wavelet denoising. *IEEE Transactions on Signal Processing*, 49(6):1146–1152, 2001.
- [32] Karen Simonyan and Andrew Zisserman. Very deep convolutional networks for large-scale image recognition, 2015.
- [33] Y. Song, Y. Zhu, and X. Du. Grouped multi-scale network for real-world image denoising. *IEEE Signal Processing Letters*, pages 1–1, 2020.
- [34] Yuzhi Wang, Haibin Huang, Qin Xu, Jiaming Liu, Yiqun Liu, and Jue Wang. Practical deep raw image denoising on mobile devices, 2020.
- [35] Jun Xu, Lei Zhang, David Zhang, and Xiangchu Feng. Multi-channel weighted nuclear norm minimization for real color image denoising, 2018.
- [36] N. Yair and T. Michaeli. Multi-scale weighted nuclear norm image restoration. In *CVPR*, pages 3165–3174, 2018.

- [37] Syed Waqas Zamir, Aditya Arora, Salman Khan, Munawar Hayat, Fahad Shahbaz Khan, Ming-Hsuan Yang, and Ling Shao. Cycleisp: Real image restoration via improved data synthesis, 2020.
- [38] Syed Waqas Zamir, Aditya Arora, Salman Khan, Munawar Hayat, Fahad Shahbaz Khan, Ming-Hsuan Yang, and Ling Shao. Learning enriched features for real image restoration and enhancement, 2020.
- [39] Richard Zhang, Phillip Isola, Alexei A Efros, Eli Shechtman, and Oliver Wang. The unreasonable effectiveness of deep features as a perceptual metric. In *CVPR*, 2018.
- [40] Yiyun Zhao, Zhuqing Jiang, Aidong Men, and Guodong Ju. Pyramid real image denoising network, 2019.

# Feature-Align Network and Knowledge Distillation for Efficient Denoising

## - Supplemental -

Lucas D. Young\*  
Jon Morton  
Xiaoyu Xiang

Fitsum A. Reda\*<sup>†</sup>  
Jun Hu  
David Liu  
Facebook Inc.

Rakesh Ranjan  
Yazhu Ling  
Vikas Chandra

### 6. Noise Modeling

Image noise originates at the Bayer RAW domain. The observed signal of a pixel is gaussianly distributed about the noiseless intensity of the pixel. Noise originates from a variety of sources, but can be broken down into two categories - signal independent noise and signal dependent noise. The variance of the gaussian distribution of signal independent noise per-pixel does not vary depending on the intensity of a pixel. The variance of signal dependent noise per-pixel is proportional to that pixel’s intensity. Read noise is a prominent example of signal independent noise and shot noise is a prominent example of signal dependent noise.

$$y \sim \mathcal{N}(\mu = x, \sigma^2 = ax + b) \quad (7)$$

Equation 7 models both signal independent noise and signal dependent noise as a single heteroscedastic gaussian, treating  $y$  as a variable whose variance is a function of the true signal  $x$ , where  $a$  and  $b$  represent the signal dependent and signal independent noise respectively [4, 34, 5]. This description of noise is only partially complete because it does not account for clipping of the signal. Due to clipping, the per-pixel distribution of a pixel is a censored gaussian distribution, and the expected variance at the low and high ends of the signal are decreased compared to Equation 7 [4]. To accurately model noise for a specific sensor, we choose realistic  $a$  and  $b$  parameters, sample the corresponding gaussian distribution for each pixel, add the noise to the ground truth image, and then clip the image.

To pick realistic  $a$ s and  $b$ s for the target sensor, we conduct an empirical analysis. In a lab-controlled lighting environment, we capture samples of frames of a color checker in a variety of lighting conditions, holding exposure time constant. We scale the image’s intensities to a 0-1 range in accord with the camera’s white and black levels. After segmenting color boxes in the checker, we approximate the

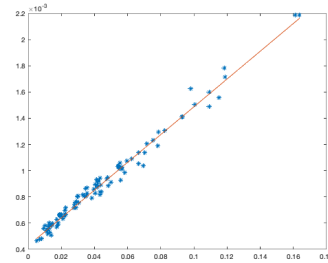


Figure 8. Example of intensity (x-axis) vs variance (y-axis) for a single image of a color checker.

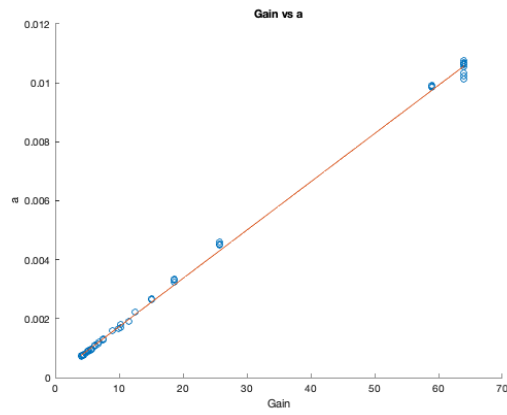
noise-free intensity of each pixel as the mean intensity of its corresponding color box. This allows us to observe the relationship between noise-free intensity and variance for each image (see Figure 9).

We use the algorithm proposed by [4] to fit Equation 7 to this plot. Note that while the images used for this analysis are clipped, the algorithm takes this discrepancy into account when fitting the theoretical unclipped noise model. This yields the parameters  $a$  and  $b$  for the image, which can be used to generate artificial noise to be subsequently added to a ground truth image and clipped.

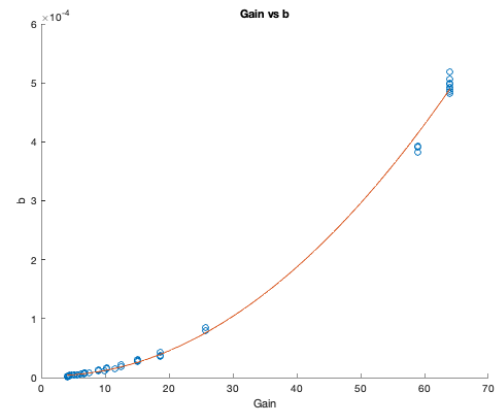
In training, we model the distribution of these  $a$  and  $b$  pairs in logarithmic space, randomly choose  $\log a$  along a uniform distribution, and then pick  $\log b$  based on a linear regression. The resulting regression is unique to each type of sensor. Our noise modeling was done for target camera’s sensor, the Sony IMX258. Since the image’s gain is known at inference, to predict the noise levels at inference we create regressions between  $a$  and gain and between  $b$  and gain. We find that a linear regression fits the relationship between  $a$  and gain and that a quadratic regression fits the relationship between  $b$  and gain. As demonstrated in [34], superior denoising performance can be achieved by having this information available to the algorithm.

\*Equal contribution.

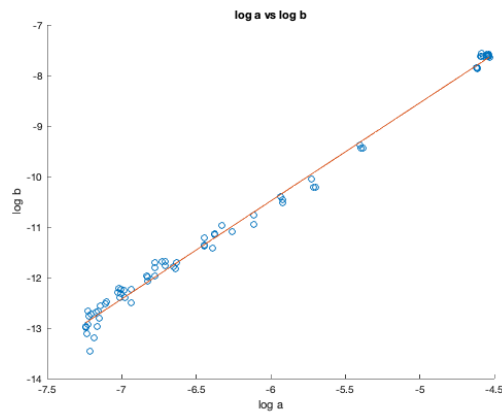
<sup>†</sup>Currently affiliated with Google.



(a) Linear regression between gain and  $a$



(b) Quadratic regression between gain and  $b$



(c) Regression between  $\log a$  and  $\log b$

Figure 9. The regressions in (a) and (b) are used to estimate noise parameters in inference. The regression in (c) is used to randomly choose noise parameters in training.